Influence of the material dielectric constant on plasma generation inside catalyst pores

Influence of the material dielectric constant on plasma generation inside catalyst pores

Yu-Ru Zhang[a,b,*], Erik C. Neyts[b] and Annemie Bogaerts[b]

[a]*Key Laboratory of Materials Modification by Laser, Ion, and Electron Beams (Ministry of Education), School of Physics and Optoelectronic Technology, Dalian University of Technology, Dalian 116024, People's Republic of China*

[b]*Research group PLASMANT, Department of Chemistry, University of Antwerp, Universiteitsplein 1, BE-2610 Wilrijk-Antwerp, Belgium*

E-mail address: yrzhang@dlut.edu.cn

Abstract

Plasma catalysis is gaining increasing interest for various environmental applications, but the crucial question is whether plasma can be created inside catalyst pores and under which conditions. In practice, various catalytic support materials are used, with various dielectric constants. We investigate here the influence of the dielectric constant on the plasma properties inside catalyst pores and in the sheath in front of the pores, for various pore sizes. The calculations are performed by a two-dimensional fluid model for an atmospheric pressure dielectric barrier discharge in helium. The electron impact ionization rate, electron temperature, electron and ion density, as well as the potential distribution and surface charge density, are analyzed for a better understanding of the discharge behavior inside catalyst pores. The results indicate that in a 100 μm pore, the electron impact ionization in the pore, which is characteristic for the plasma generation inside the pore, is greatly enhanced for dielectric constants below 300. Smaller pore sizes only yield enhanced ionization for smaller dielectric constants, i.e., up to ε_r = 200, 150 and 50 for pore sizes of 50 μm, 30 μm and 10 μm. Thus, the

most common catalyst supports, i.e., Al_2O_3 and SiO_2, which have dielectric constants around ε_r = 8-11 and 4.2, respectively, should allow more easily that microdischarges can be formed inside catalyst pores, even for smaller pore sizes. On the other hand, ferroelectric materials with dielectric constants above 300 never seem to yield plasma enhancement inside catalyst pores, even not for 100 μm pore sizes. Furthermore, it is clear that the dielectric constant of the material has a large effect on the extent of plasma enhancement inside the catalyst pores, especially in the range between ε_r = 4 and 200. The obtained results are explained in detail based on the surface charge density at the pore walls, and the potential distribution and electron temperature inside and above the pores. The results obtained with this model are important for plasma catalysis, as the production of plasma species in catalyst pores might affect the catalyst properties, and thus improve the applications of plasma catalysis.

Keywords

Microdischarge formation; Catalyst pores; Dielectric constant; Pore size; Fluid simulation;

1. Introduction

Plasma catalysis is increasingly gaining attention in recent years, for various environmental applications, such as gaseous pollutant removal, hydrocarbon reforming and the conversion of greenhouse gases into value-added chemicals[1-6]. In single-stage plasma catalysis systems, the interaction between the plasma and the catalyst is rather complicated, and this directly influences the performance of plasma catalysis. For instance, the reactants generated in the plasma phase arrive at the catalyst surface, affecting the electronic and chemical properties of the catalyst, i.e., the adsorption probability, oxidation state, as well as the work function [7-12]. In addition, the presence of a catalyst in the plasma zone may enhance the electric field, change the discharge type, and thus in turn affect the physical and chemical properties of the plasma [13-17].

The electric field distribution near the catalyst surface is one of the most important parameters in plasma catalysis, as it directly affects the plasma generation, and in turn modifies the catalyst operation [18-26]. Indeed, by including a catalyst in the plasma volume, the roughness and the dielectric constant of the catalyst will modify the electric field in the vicinity of the catalyst. More specifically, the electric field can be enhanced due to the polarization effect and the charge accumulation on the dielectric surface, especially on localized spots with large curvature. This modified electric field directly affects the electron energy distribution function, and therefore the electron impact reaction rates. This, in turn, changes the chemical composition of the plasma. A variety of reactive species, including neutral species, ions and electrons, arrive at the catalyst surface, leading to a significant change in the surface structure and morphology, and hence, the catalytic activity.

In the case of a porous catalyst surface (or porous catalyst support), the enhanced electric field near the catalyst pores plays an important role in the generation of plasma species, as well as in the microdischarge formation inside the pore [27-33]. Holzer et al. [27, 28]

experimentally revealed the presence of short-lived oxidants inside catalyst pores, and they concluded that these species might be produced in the interior of porous catalysts, due to the stronger electric field there than in the bulk plasma. In addition, the same authors indicated that the energy input in a ferroelectric packed-bed reactor was higher than in an empty reactor, due to the formation of microdischarges [29]. Hensel et al. [30-32] studied the microdischarges inside porous ceramic material. They observed a transition in discharge mode, i.e., from surface discharge to microdischarge, when the pore size and the applied voltage increase. In our previous work [33], we used a two-dimensional fluid model to investigate the microdischarge formation inside catalyst pores for various pore sizes and applied voltages. By means of detailed modeling, we demonstrated for the first time that the ionization mainly takes place inside catalyst pores because of the strong electric field there, with pore sizes above 10 μm.

In plasma catalysis, the electric field enhancement is governed by the dielectric constant of the (catalytic or support) material, and this has been investigated both experimentally [29, 34, 35] and theoretically [36-39]. Mizuno et al. [34] performed measurements in a dielectric barrier discharge (DBD) with five different kinds of pellets, showing that the initiation voltage of the partial discharge was lower and the discharge power was higher, in the case of high dielectric constant pellets. Roland et al. [35] studied the influence of the packed-bed materials on the performance of non-thermal plasmas for the removal of organic air pollutants. They proved that the introduction of glass beads ($\varepsilon_r = 5$) had no remarkable influence on the oxidation of toluene, whereas the oxidation was significantly enhanced by ferroelectric packed-bed materials ($\varepsilon_r \approx 2000$). Subsequently, the same authors [29] indicated that a high removal degree as well as a high CO_2 selectivity was achieved when the reactor was filled with both ferroelectric $BaTiO_3$ (with high dielectric constant) and catalytically active $LaCoO_3$ (with low dielectric constant), compared with the performance in case of the individual

packing materials. Takaki et al. [36] simulated a ferroelectric packed bed barrier discharge in nitrogen, and concluded that the electron density and electron temperature increased with the dielectric constant of the pellets, due to the enhanced electric field. Jo et al [37] revealed that the presence of a conductive Pt catalyst on the surface of Al_2O_3 beads distorted and lowered the electric field, especially near the grounded electrode. Since the dissociation of methane in non-thermal plasmas is mainly activated by collisions of electrons with energies above 9 eV, the lower electric field decreased the electron impact reaction rate, and accordingly the methane conversion rate. Recently, Van Laer et al. [38] studied the plasma behavior in a packed bed DBD by means of a 2D fluid model, and clearly showed the electric field enhancement due to polarization of the packing beads. Likewise, Zhang et al. [39] used a two-dimensional particle-in-cell/Monte Carlo (PIC/MC) model to describe a packed bed DBD reactor, focusing on the electric field distribution for different dielectric constants. They reported that the electric field became stronger and the electron density was higher for a larger dielectric constant, because the dielectric material was more effectively polarized.

It is thus clear that amongst the various properties of the catalyst and support material, their dielectric constant in particular is a very important factor for plasma catalysis, as it determines the electric field distribution and the plasma generation, and the plasma species inside the catalyst pores thus affect the catalyst active surface that is available for the catalytic reactions. The most common catalysts or support materials can be categorized into ferroelectric materials (e.g., $BaTiO_3$ ($\varepsilon_r \approx 10000$), $SrTiO_3$ ($\varepsilon_r \approx 300$) and $CaTiO_3$ ($\varepsilon_r \approx 200$)), semiconductors (e.g., TiO_2 ($\varepsilon_r = 40\sim100$) and WO_3 ($\varepsilon_r = 10\sim20$)), oxides (e.g., ZrO_2 ($\varepsilon_r = 22\sim25$), CeO_2 ($\varepsilon_r \approx 24$), γ-Al_2O_3 ($\varepsilon_r = 8\sim11$) and SiO_2 ($\varepsilon_r = 4.2$)), and zeolites ($\varepsilon_r = 1.5\sim5$) [19,29]. In order to improve the plasma catalysis applications, a better understanding of the influence of the dielectric materials on the electric field enhancement, as well as on the plasma generation inside pores, is crucial. Indeed, although the studies mentioned above

investigated the electric field enhancement ***near*** dielectric materials, a detailed study on the plasma behavior ***inside*** catalyst pores, for materials with different dielectric constants, has not yet been performed. In the present work, we therefore investigate the plasma properties inside and in front of catalyst pores, for various dielectric constants. With this study, we aim to obtain more insight into the mechanisms behind the electric field enhancement by the catalyst or support material with different dielectric constants, as well as the effect on the plasma behavior.

2. Description of the model

We developed a two-dimensional fluid model within the COMSOL simulation software [40], which has already been described in [33]. Therefore, only a short description is included here for completeness. The plasma behavior is described by a set of coupled equations, i.e., the continuity equations for the electron density, heavy species densities and mean electron energy. We assumed a constant temperature of the heavy particles of 300 K. Moreover, the Poisson equation is solved to calculate the electrostatic field, by using the densities of various charged plasma species.

The DBD configuration is adopted in this work (see Fig. 1), as it has been most commonly used for plasma catalysis [33, 36-39]. An AC source with a voltage of 20 kV and a frequency of 25 kHz is applied to the top electrode, which is covered by a 1 mm thick layer of alumina (ε_r = 9). The bottom electrode is grounded, and covered by different dielectric materials, i.e., with dielectric constants in the range of 4-1000, leaving a discharge gap of 2 mm. The pores, with a fixed aspect ratio of 0.52, are always assumed to be vertical in the bottom dielectric plate, and the pore size indicates the diameter of the pore. In order to reduce the computational cost, we only focus on the plasma behavior near the pore, and the computation domain is limited to a small section of the discharge, i.e., 0.2 mm.

Although plasma catalysis is in reality typically performed in reactive gases, we adopt helium as the working gas in this model. This is because on one hand, it typically forms a homogeneous instead of a filamentary discharge in a DBD [41], which is easier to describe with a fluid model. On the other hand, the simple chemistry of this noble gas could help to limit the computation time. The insights gained from this work provide a more fundamental understanding of the influence of the dielectric constant on the electric field enhancement, which in turn is quite helpful for future research with more complex molecular gases.

The model includes six species: electrons (e), positive ions (He^+, He_2^+), helium ground state atoms (He), helium dimers (He_2^*) and a combined metastable level (He^*) which consists of He (2^1S) and He (2^3S). The different species interact with each other, and the chemical reactions considered in this work are listed in Table I [38, 42]. For the first five reactions, the rate coefficients are calculated from energy-dependent collision cross sections by the BOLSIG+ code [43]. It also calculates the transport coefficients for the electrons, as a function of mean energy. The rate coefficients of the other reactions are taken from literature. The mobilities of He^+ and He_2^+ are taken from [44], and the Chapman-Enskog equation is used to calculate the diffusion coefficients for the neutral species.

The computational mesh structure is very important, as it affects the stability and efficiency of the calculation. Quadrilateral meshing is used across the whole geometry, except near and inside the pore, where triangular meshing is adopted. Near the top and bottom dielectric plates, the mesh is refined, and the mesh size decreases from about 15 μm in the bulk region to about 2 μm, for better solving the sheath formation. Inside the pore, the mesh size is limited to 0.5 μm.

Table 1: Chemical reactions included in the model, where T_e is the electron temperature in eV, T_g is the gas temperature in eV, and T_g' is the gas temperature in K.

No.	Reaction	Rate Coefficient	Reference
R1	$e + He \rightarrow He + e$	From cross-section	45
R2	$e + He \rightarrow He^* + e$	From cross-section	45
R3	$e + He^* \rightarrow He + e$	From cross-section	43
R4	$e + He \rightarrow He^+ + 2e$	From cross-section	45
R5	$e + He^* \rightarrow He^+ + 2e$	From cross-section	45
R6	$e + He_2^* \rightarrow 2He + e$	3.8×10^{-9} cm^3 s^{-1}	46, 47
R7	$2e + He^+ \rightarrow He^* + e$	$6.0 \times 10^{-20} (T_e/T_g)^{-4.4}$ cm^6 s^{-1}	47
R8	$2e + He_2^+ \rightarrow He^* + He + e$	$4.0 \times 10^{-20} (T_e/T_g)^{-1}$ cm^6 s^{-1}	47
R9	$e + He_2^+ + He \rightarrow He^* + 2He$	$5.0 \times 10^{-27} (T_e/T_g)^{-1}$ cm^6 s^{-1}	47
R10	$2e + He_2^+ \rightarrow He_2^* + e$	$4.0 \times 10^{-20} (T_e/T_g)^{-1}$ cm^6 s^{-1}	47
R11	$e + He_2^+ + He \rightarrow He_2^* + He$	$5.0 \times 10^{-27} (T_e/T_g)^{-1}$ cm^6 s^{-1}	47
R12	$e + He_2^* \rightarrow He_2^+ + 2e$	$9.75 \times 10^{-10} T_e^{0.71} e^{-3.4/Te}$ cm^3 s^{-1}	47
R13	$e + He^+ + He \rightarrow He^* + He$	$1.0 \times 10^{-26} (T_e/T_g)^{-2}$ cm^6 s^{-1}	47
R14	$e + He_2^+ \rightarrow He_2^*$	$5.0 \times 10^{-9} (T_e/T_g)^{-1}$ cm^3 s^{-1}	47
R15	$He^* + He^* \rightarrow He_2^+ + e$	$2.03 \times 10^{-9} (T_g/0.025)^{0.5}$ cm^3 s^{-1}	47
R16	$He^* + He^* \rightarrow He^+ + He + e$	$8.7 \times 10^{-10} (T_g/0.025)^{0.5}$ cm^3 s^{-1}	47
R17	$He^+ + 2He \rightarrow He_2^+ + He$	$1.4 \times 10^{-31} (T_g/0.025)^{-0.6}$ cm^6 s^{-1}	47
R18	$He^* + 2He \rightarrow He_2^* + He$	$8.1 \times 10^{-36} T_g$, $e^{-650/Tg'}$ cm^6 s^{-1}	47
R19	$He_2^* + He^* \rightarrow He^+ + 2He + e$	$2.03 \times 10^{-9} (T_g/0.025)^{0.5}$ cm^3 s^{-1}	47
R20	$He_2^* + He^* \rightarrow He_2^+ + He + e$	$8.7 \times 10^{-10} (T_g/0.025)^{0.5}$ cm^3 s^{-1}	47
R21	$He_2^* + He_2^* \rightarrow He^+ + 3He + e$	$2.03 \times 10^{-9} (T_g/0.025)^{0.5}$ cm^3 s^{-1}	47
R22	$He_2^* + He_2^* \rightarrow He_2^+ + 2He + e$	$8.7 \times 10^{-10} (T_g/0.025)^{0.5}$ cm^3 s^{-1}	47
R23	$He_2^* + He \rightarrow 3He$	4.9×10^{-22} cm^3 s^{-1}	46

3. Results and discussion

The dielectric constant of the catalytic or support material was proven to have a significant influence on the enhancement of the electric field, which in turn affects the performance of plasma catalysis [29, 34-39]. In order to gain more insight, we investigate the ionization rate, electron temperature, plasma density and electric potential distribution inside and above the catalyst pores, as well as the surface charge density, for various dielectric constants, i.e., in the range of 4-1000. First, the calculations are performed for a fixed pore size (i.e., diameter of 100 μm and depth of 194 μm).

3.1 Ionization rate and electron temperature inside and above the pores

Fig. 2 shows the calculated time-averaged electron impact ionization rate inside and above the pores (cf. Fig. 1), for various dielectric constants, i.e., 25, 300, 400 and 1000. The results obtained for other dielectric constants are not shown here, but the data for $\varepsilon_r \leq 200$ are similar to those for $\varepsilon_r = 25$, while the behavior for $\varepsilon_r = 500$ is similar to the case of $\varepsilon_r = 1000$, except for different absolute values. Note that a different color scale is used for $\varepsilon_r = 25$, to show the differences more clearly.

It is obvious from Fig. 2(a) that when $\varepsilon_r = 25$ (and more in general for $\varepsilon_r \leq 200$), the ionization mainly takes place inside the catalyst pore. Moreover, the maximum ionization rate in the pore is about three orders of magnitude higher than in the bulk region, which is a clear evidence for microdischarge formation inside the pore. When the dielectric constant of the bottom dielectric plate increases to 300 (Fig. 2(b)), the ionization rate inside the pore decreases, whereas the value in the sheath becomes higher. However, the maximum still appears inside and above the pore. As the dielectric constant increases further to 400 (Fig. 2(c)), the ionization rate profile becomes strikingly different. The ionization rate inside the pore decreases significantly, with the maximum appearing in the sheath near the bottom

dielectric plate, indicating that for this higher dielectric constant no microdischarge can be formed anymore inside the pore. Finally, when $\varepsilon_r = 1000$, the ionization rate inside the pore is about two orders of magnitude lower than in the sheath. Besides, the maximum in the sheath exhibits somewhat higher absolute values than in the cases with lower dielectric constants (cf. Fig. 2(d)), due to the higher electron temperature there (as will be discussed below).

The ionization rate profiles are largely determined by the electron temperature, so the effect of the dielectric constant on the spatial distribution of the electron temperature is presented in Fig. 3. It is clear from Fig. 3(a) that when $\varepsilon_r = 25$ (and more in general when $\varepsilon_r \leq 200$), the electron temperature reaches its minimum in the bulk region, and it increases significantly inside the pore, which is responsible for the high ionization rate inside the pore (see Fig. 2(a)). As the dielectric constant increases to 300, the electron temperature in the sheath near the bottom dielectric increases to about 4.3 eV, whereas it decreases inside the pore, but the absolute value inside the pore is still higher than in the sheath near the bottom dielectric, as shown in Fig. 3(b). This explains why the maximum ionization rate takes place near and inside the pore, as is obvious from Fig. 2(b). As the dielectric constant increases further to 400, the electron temperature inside the pore decreases further, and the absolute value is slightly lower than in the sheath in front of the bottom dielectric plate. Especially when $\varepsilon_r = 1000$, the electron temperature in the sheath near the bottom dielectric is about 2 eV higher than inside the pore (see Fig. 3(d)), and this gives rise to the higher ionization rate there (see Fig. 2(d)).

To better visualize the effect of the dielectric constant on the plasma behavior near and inside the catalyst pore, the ionization rate and electron temperature, as well as the electron density and total ion density distributions along the vertical centerline are plotted in Fig. 4, for various dielectric constants. Note that the negative y-values, y = 0 mm and y = 2 mm correspond to the bottom of the pore, the top of the pore and the top dielectric layer, respectively.

The ionization rate exhibits two peaks for all dielectric constants investigated, i.e., one peak in the sheath in front of the top dielectric plate, and another peak either in the sheath in front of the bottom dielectric plate or inside the pore (see Fig. 4(a)). In all cases, the value in the bulk region is very low, due to the low electron temperature there, i.e., lower than 1 eV (Fig. 4(b)). When $\varepsilon_r = 4$, two asymmetric peaks are observed, i.e., one in the sheath near the top dielectric plate and the other inside the pore, and the maximum ionization rate inside the pore is about 6 times higher than in the sheath near the top dielectric (i.e., 1.2×10^{25} $m^{-3}s^{-1}$ vs 2.0×10^{24} $m^{-3}s^{-1}$). This is clear evidence for the enhanced plasma generation inside the pore, and it can be understood by examining the electron temperature distribution at $\varepsilon_r = 4$. Indeed, the peak value is 6.3 eV inside the pore, whereas it is 3.4 eV in the sheath near both dielectric plates.

When the dielectric constant increases to 50, the ionization rate shows a similar behavior. Both the maxima inside the pore and in the sheath near the top dielectric plate increase with ε_r, and the ionization mainly takes place inside the pore (with maximum values around 2.9×10^{25} $m^{-3}s^{-1}$), as was also clear from Fig. 2(a). At a dielectric constant of 200, the peak value in the sheath increases slightly due to the increasing electron temperature, whereas the maximum inside the pore decreases to about 1.7×10^{25} $m^{-3}s^{-1}$, but the ionization inside the pore still plays a dominant role in the discharge. Moreover, the ionization rate outside the pore near the bottom dielectric is significantly enhanced to about 1.0×10^{25} $m^{-3}s^{-1}$.

Increasing the dielectric constant further to $\varepsilon_r = 300$, the ionization rate inside the pore now decreases more rapidly to about 4.5×10^{24} $m^{-3}s^{-1}$, and the value near the bottom dielectric becomes comparable to the value inside the pore (as was also clear from Fig. 2(b)), as well as to the value in the sheath near the top dielectric. Thus, the ionization in the sheaths is equally important as the ionization inside the pore under this condition.

As the dielectric constant is further increased, the ionization rate inside the pore continues to decrease, with a maximum of about 9.2×10^{23} $m^{-3}s^{-1}$ at $\varepsilon_r = 400$, and even down to 1.1×10^{23} $m^{-3}s^{-1}$ at $\varepsilon_r = 1000$. The latter is a decrease by more than two orders of magnitude compared to the case of $\varepsilon_r = 50$-200. At these high values for the dielectric constant of $\varepsilon_r = 400$ and $\varepsilon_r = 1000$, the maxima only appear in the sheaths, which indicates that the discharge behavior is dominated by ionization in the sheaths, as was also clear from Figs. 2(c) and 2(d). Note that the ionization rate inside the pore thus first increases with dielectric constant, and then it decreases, which will be discussed in detail below.

The evolution of the electron temperature with dielectric constant is illustrated in Fig. 4(b). When $\varepsilon_r = 4$, the electron temperature exhibits two maxima, i.e., inside the pore and in the sheath near the top dielectric, and the value inside the pore is about 3 eV higher than in the sheath because of the strong electric field there (see below), which indicates the remarkable influence of the pore on the plasma characteristics. As the dielectric constant increases, the electric field in the sheath becomes stronger, leading to a higher electron temperature, and accordingly more ionization (see Fig. 4(a) above), whereas a reverse trend is observed inside the pore. Indeed, the electron temperature inside the pore is more or less constant (around 6.3 eV) up to a dielectric constant of 50, but higher values of the dielectric constant yield a significant drop in the electron temperature, down to a value of 3.4 at $\varepsilon_r = 1000$, which is slightly lower than in the sheath above the pore. Note that the electron temperature in the sheath near the bottom dielectric is higher above the dielectric material than right above the pore (i.e., up to 5.6 eV; cf Fig. 3(d)), implying that the plasma generation in the sheath plays a dominant role under this condition. This can be explained by the weak electric field inside the pore, which is clear from the potential distribution (as will be discussed below).

3.2 Plasma species densities inside and above the pores

The influence of the dielectric constant on the electron density profiles is presented in Fig. 4(c). When $\varepsilon_r = 4$, the maximum of the electron density appears in the bulk region, and it decreases clearly towards the top dielectric. However, the electron density exhibits a strikingly different behavior near the bottom dielectric, i.e., it first increases near the pore, and then it decreases to low values at the bottom of the pore, leading to an asymmetric distribution along the vertical direction. Although the ionization mainly takes place inside the pore, the electron density near the pore is higher than inside the pore, due to the strong electric field, which pushes the electrons back into the bulk plasma (see below). As the dielectric constant becomes larger (i.e., in the range of 4-50), the electron density shows a similar behavior, except that the peak near the pore becomes more pronounced. Indeed, at $\varepsilon_r = 50$, the electron density near the pore is higher than in the bulk region. As the dielectric constant increases to 200, this peak becomes less evident, due to the reduced ionization rate inside the pore caused by the lower electron temperature (see above). When the dielectric constant is above 300, the peak near the pore disappears, and the electron density decreases monotonically from the bulk region to the bottom of the pore. Under this condition, the electron density inside the pore is only slightly enhanced, indicating the limited influence of the pore on the plasma properties.

The evolution of the ion density profiles with changing dielectric constant is quite different, as is clear from Fig. 4(d). The ion density distribution in the bulk region is similar to the electron density, but it is characterized by two maxima, i.e., one inside or above the pore (depending on the value of ε_r) and the other in the sheath near the top dielectric, because of the enhanced ionization rate in both regions (see above). The ion density in the sheath near the top dielectric slightly increases with ε_r, whereas the value inside the pore first increases up to $\varepsilon_r = 25$, and then decreases, following the behavior of the ionization rate. Indeed, when the dielectric constant is below or equal to 300, the maximum ion density appears inside the pore, indicating that the production of plasma species inside the pore is remarkably enhanced.

When ε_r = 400 or above, the ion density profiles are characterized by two similar peaks in the sheaths near the top and bottom dielectric, and the pore only affects the ion density to a limited extent.

A similar behavior is observed for the other plasma species, i.e., $He^*$and He_2^* (not shown here). When the dielectric constant is below or equal to 50, the He^* density is characterized by two maxima, and the value inside the pore is around 1.5-1.8 times higher than in the sheath in front of the top dielectric, as shown in our previous work [33]. When the dielectric constant increases to higher values, the He^* density inside the pore decreases rapidly, and becomes even slightly lower than in the sheath near the top dielectric at ε_r = 200, whereas it is significantly enhanced in the sheath near the bottom dielectric. At ε_r = 300, the values inside the pore and in the sheath near the bottom dielectric are comparable, while at ε_r = 400 and ε_r = 1000, the He^* density inside the pore is negligible, and two similar peaks are observed in both sheaths in front of the top and bottom dielectric plates.

The evolution of the He_2^* density with dielectric constant is similar, except that its density distribution is dominated by a maximum in the sheath near the top dielectric when ε_r = 4 and ε_r = 9, and the value inside the pore is only slightly higher than in the sheath near the bottom dielectric. As the dielectric constant rises, a peak in the density profile in the sheath near the bottom dielectric appears, and it becomes comparable to the value inside the pore at ε_r = 25, while at ε_r = 400 and ε_r = 1000, the He_2^* density becomes equal to that in the sheath near the top dielectric, whereas the density inside the pore is negligible.

3.3 Electric potential distribution inside and above the pores

For a better understanding of the different plasma behavior due to the different dielectric constants of the catalytic or support material, we illustrate in Fig. 5 the time-averaged potential distributions for the same dielectric constants as in Figs. 2 and 3 above. Again, the

results obtained for $\varepsilon_r \leq 200$ are similar to those for $\varepsilon_r = 25$, and they gradually evolve to that for $\varepsilon_r = 300$, while the behavior for $\varepsilon_r = 500$ is similar to the case of $\varepsilon_r = 400$.

When $\varepsilon_r = 25$, the potential far away from the pore is quite uniform, which is clear from the straight contour lines, as shown in Fig. 5(a), indicating that the discharge behavior is not affected here by the presence of the pore. The potential in the sheath decreases slightly by about 15 V, i.e., from 105 V (at y = 0.1 mm) to about 90 V at the surface of the bottom dielectric plate (or top of the pore). However, inside the pore, the potential drops strikingly to about -17 V at the bottom. The larger potential drop inside the pore gives rise to a stronger axial electric field, and thus to a higher electron temperature and ionization rate, as was clear from Figs. 2(a) and 3(a) above.

As the dielectric constant increases to 300, the potential drop inside the pore is quite similar and only slightly lower, i.e., from 90 V at the top of the pore to about -12 V at the bottom of the pore. However, in the sheath near the bottom dielectric, the potential drop is more pronounced, i.e., about 45 V, from 135 V at y = 0.1 mm to about 90 V at the top of the pore, as is clear from Fig. 5(b). This is because for a larger dielectric constant, the dielectric material becomes more effectively polarized, giving rise to an enhanced potential drop or electric field there. As a result, the electrons gain more energy, leading to a higher electron temperature in the sheath (see Fig. 3(b)), and resulting in more ionization there (see Fig. 2(b)).

When the dielectric constant is equal to $\varepsilon_r = 400$, the potential drop in the sheath increases further to about 60 V (i.e., from 135 V at y = 0.1 mm to 75 V at y = 0 mm), while the potential drop inside the pore is slightly reduced, i.e., from 75 V at the top to -9 V at the bottom; see Fig. 5(c).

When $\varepsilon_r = 1000$, the potential distribution is remarkably different, especially inside the pore. Indeed, the potential again mainly drops in the sheath, from about 80 V at y = 0.1 mm to 30 V at the top of the pore, as is obvious from Fig. 5(d), but it only decreases slightly from 30 V to

-1 V inside the pore. The large gradient in the sheath is responsible for the pronounced electric field enhancement, and accordingly the high electron temperature (see Fig. 3(d)), and this also explains the high ionization rate in the sheath, as shown in Fig. 2(d), while the electric field, and thus the electron temperature and ionization rate are very low inside the pore.

3.4 Surface charge density at the bottom dielectric and pore walls

The surface charge density at the bottom dielectric and at the pore walls is shown in Figure 6, for various dielectric constants. To clearly show the different behavior, the surface is divided into 5 regions, i.e., the dielectric surface outside the pore (regions A and E), the surface of the sidewalls in the pore (regions B and D), and the surface at the bottom of the pore (region C).

When the dielectric constant is below or equal to 200, the surface charge density exhibits a similar distribution. A positive charge is accumulated on the dielectric surface outside the pore (i.e., regions A and E). This is attributed to the electric field in the sheath, which directs downwards, pushing more ions towards the bottom dielectric and accumulating there. Moving closer to the pore, the charge density decreases and reaches a negative value at the edge of the pore (i.e., the intersection between regions A-B and D-E). However, the charge density becomes positive again at the sidewalls in the top half of the pore (i.e., position $\in$ [0.06, 0.17] mm and position $\in$ [0.36, 0.47] mm). This is because sheaths form in the horizontal direction, and the electric field along the horizontal (x) direction accelerates the positive ions towards the sidewalls. Moreover, in the top half of the pore, the sidewalls are not very steep. Therefore, the ions are also pushed towards the sidewalls by the vertical electric field. Deeper inside the pore (i.e., the bottom half of regions B and D), the sidewalls become more vertical, and the surface charge density drops to negative values. This is because the vertical electric field is much stronger than the horizontal electric field in this region, and this limits the migration of

positive ions towards the sidewalls. Hence, the influence of the thermal motion of the charged species on the surface charge density becomes more important than migration due to the electric field. Since the electron thermal velocity is much higher than the ion thermal velocity, a negative charge accumulation takes place at the sidewalls in the bottom half of the pore. At the bottom of the pore, i.e., region C, although some ions are accumulated on the surface due to the vertical electric field, the thermal motion of the electrons is again dominant, due to the higher electron temperature and electron density. Therefore, negative charges are accumulated at the bottom of the pore, explaining the more significant negative surface charge density. This negative surface charge density at the bottom of the pore can explain the strong potential drop inside the pore, illustrated in Fig. 5(a).

As the dielectric constant increases to 300 and 400, the surface charge density still exhibits a similar distribution, except for higher absolute values. For instance, at $\varepsilon_r = 4$ and $\varepsilon_r = 25$, the charge density outside the pore is about 1.7×10^{-5} C.m^{-2} and 3.5×10^{-5} C.m^{-2}, respectively (not visible in this figure), and it increases by more than two orders of magnitude at $\varepsilon_r = 400$. A similar behavior is also observed at the bottom of the pore, i.e., the absolute value of the negative surface charge density increases from about 2.2×10^{-5} C.m^{-2} at $\varepsilon_r = 4$ to 1.3×10^{-3} C.m^{-2} at $\varepsilon_r = 400$. These larger surface charge densities arise because the dielectric material is more effectively polarized for a larger dielectric constant. A stronger polarization gives rise to a stronger local electric field, or in other words a stronger potential drop above the bottom dielectric, and thus, this leads to more positive charge accumulation at the bottom dielectric outside the pore. Inside the pore, the electric field is slightly enhanced when the dielectric constant increases from 4 to 25. However, when the dielectric constant increases further, the influence of the polarization of the left sidewall counteracts that of the right sidewall, and therefore the electric field becomes weaker, leading to a reduced flow by migration. Consequently, the thermal motion of the electrons, rather than the migration of the positive

ions, has a dominant effect, resulting in more negative charge accumulation for larger dielectric constants.

Especially at $\varepsilon_r = 1000$, this counteraction between left and right sidewalls becomes more obvious, and a relatively uniform potential distribution inside the pore is observed (see Fig. 5(d)). The electric field becomes much weaker, and the axial electric field at the bottom of the pore is even one order of magnitude lower than at $\varepsilon_r = 4$ (not shown here). Therefore, the isotropic electron transport governs the surface charge density, generating an almost uniform charge density distribution inside the pore. The lower absolute value of the surface charge density is caused by the lower electron density inside the pore under this condition. Furthermore, more pronounced positive peaks in the surface charge density are observed at the edge of the pore, i.e., at positions of about 0.05 mm and 0.15 mm, due to the stronger local electric field, which is directed towards the surface and causes a significant positive charge accumulation at the edges of the pore.

3.5 Different behavior for different pore sizes

Since it was demonstrated before that the pore size plays an important role in the formation of a microdischarge inside the pore [30-33], the influence of the dielectric constant on the discharge behavior may be different for smaller pores. Therefore, we have also studied the evolution of the various plasma properties with changing dielectric constant, for smaller pores (up to 10 μm). Figure 7 illustrates the electron impact ionization rate, electron temperature and total ion density inside the pore as a function of dielectric constant for various pore sizes, i.e., 10 μm, 30 μm, 50 μm and 100 μm (solid lines with close symbols). For comparison, also the values in the sheath near the top dielectric are illustrated (dashed lines with open symbols). Note that the plasma properties plotted in Fig. 7 are averaged over the vertical centerline.

In the 100 μm pore, the averaged ionization rate first increases with rising dielectric constant, from $\varepsilon_r = 4$ to $\varepsilon_r = 50$, then decreases rapidly by more than one order of magnitude

towards $\varepsilon_r = 400$, and finally it decreases slightly for still higher dielectric constants (see Fig. 7(a)). This can be understood by examining the evolution of the electron temperature in Fig. 7(b). The averaged electron temperature inside the pore is the highest for low dielectric constant, and reaches it maximum at $\varepsilon_r = 25$, due to the enhanced electric field, as discussed above. This explains the maximum in the ionization rate, and thus also in the ion density at $\varepsilon_r = 25$ (Fig. 7(c)). When the dielectric constant increases from 25 to 50, the electron temperature becomes slightly lower, because the power absorption from the electric field is limited, whereas the ionization rate shows a slight increase. This is because the electric field becomes slightly weaker at $\varepsilon_r = 50$, and therefore, less electrons are pushed out of the pore, thus there are more electrons available (cf. Fig. 4(c)) to ionize neutral species inside the pore. However, although the ionization rate at $\varepsilon_r = 50$ is slightly higher than at $\varepsilon_r = 25$, a lower ion density is observed, because somewhat more ions are lost due to the enhanced electron-ion recombination at the somewhat lower electron temperature. As the dielectric constant becomes larger, the electron temperature decreases from about 5.5 eV at $\varepsilon_r = 50$ to 4.7 eV at $\varepsilon_r = 400$, and this lower electron temperature yields a significant drop in the ionization rate coefficient by more than one order of magnitude. Therefore, both the averaged ionization rate and the averaged ion density decrease dramatically from $\varepsilon_r = 50$ to $\varepsilon_r = 400$. When the dielectric constant increases further, both the electron impact ionization rate and ion density continue to decrease to low values. The low ion density inside the pore for these large dielectric constants, i.e., lower than the values inside the sheath in front of the top dielectric (cf. dashed line in Fig. 7(c)), indicates that no discharge enhancement takes place inside the catalyst pore in this case.

A similar evolution of the averaged ionization rate, electron temperature and total ion density with changing dielectric constant is also observed for the 30 μm and 50 μm pores, except for the absolute values. Indeed, the electron temperature in the smaller pores is higher

than in the larger pores, for a dielectric constant below 100, because the electric field enhancement inside the pore is more pronounced for smaller pore sizes [33], and this gives rise to the higher electron temperature and thus also a higher ionization rate inside the 50 μm and 30 μm pores (Figs. 7(a) and 7(b)). However, the ion density exhibits a monotonic increase with pore size (Fig. 7(c), because of the limited effective region for ionizationin the smaller pores, which accordingly limits the plasma generation. Moreover, for dielectric constants above 150, the electron temperature is higher in the larger pores than in the smaller pores, due to the stronger electric field. Indeed, the electric field inside the pore becomes somewhat weaker for larger dielectric constants, due to the counteraction of the polarization of both sidewalls, as mentioned above. In the smaller pores, the distance between the two sidewalls (i.e., the diameter of the pore) is smaller, indicating that the counteraction becomes significant even for a small dielectric constant. Therefore, the drop in electric field with rising dielectric constant is more remarkable in the smaller pores, leading to the faster drop in the electron temperature, as is obvious from Fig. 7(b).

The influence of the dielectric constant on the plasma properties in the 10 μm pore is different from that in the larger pores. More specifically, the electron impact ionization rate decreases significantly with rising dielectric constant, due to the similar behavior of the electron temperature, even for small dielectric constants. Indeed, inside the10 μm pore, the distance between the two sidewalls is limited, resulting in a more pronounced decreasing trend of the electric field with rising dielectric constant. Therefore, a rapid drop of the ionization rate and thus also of the ion density is observed. As the dielectric constant becomes larger than 50, both the ionization rate and the electron temperature continue to decrease, whereas the ion density shows a different trend. The averaged ion density inside the pore increases slightly above $\varepsilon_r = 50$, and the value at $\varepsilon_r = 1000$ is even higher than at $\varepsilon_r = 25$, because less ions are lost at the walls when the electric field is weaker. Indeed, the loss of ions

at the walls due to migration at $\varepsilon_r = 1000$ is more than one order of magnitude lower than at $\varepsilon_r = 50$.

As mentioned above, the averaged ionization rate, electron temperature and ion density in the sheath near the top dielectric are also plotted as a function of the dielectric constant in Fig. 7 for various pore sizes (dashed lines and open symbols), to compare with the evolution of the plasma properties inside the pores. It is clear from Fig. 7 that the plasma properties in the sheath near the top dielectric for the various pore sizes are nearly identical, which is not unexpected as the pore does not really affect the plasma at such a large distance. The ionization rate, as well as the electron temperature and the total ion density, increase monotonically with the dielectric constant up to $\varepsilon_r = 200$, and then they remain more or less constant for larger dielectric constants. By comparing the ionization rate inside the pore with that in the sheath (see Fig. 7(a)), it is clear that the ionization mainly takes place inside a 100 μm pore when the dielectric constant is below or equal to 300. Above this value, the ionization in the sheath dominates the discharge. The transition points for the 50 μm, 30 μm and 10 μm pores are $\varepsilon_r = 200$, $\varepsilon_r = 150$ and $\varepsilon_r = 50$, respectively. In other words, the plasma generation inside the larger pores is enhanced for a wider range of dielectric constants, i.e., up to $\varepsilon_r = 300$ (which is the typical value for $SrTiO_3$; see Introduction) for a 100 μm pore, while the plasma enhancement in smaller pores is limited only to lower dielectric constants, i.e., below $\varepsilon_r = 50$ (which is a typical value for TiO_2) for a 10 μm pore. In general, a dielectric constant above 300, which is characteristic for ferroelectric materials, never seems to give plasma enhancement inside the pores, even not for 100 μm pore sizes. Although some experiments are performed in discharges with different ferroelectric packed-bed materials, the plasma behavior inside the pores has not yet been studied for materials with different dielectric constants, and it might be significantly different from the behavior near packing beads. This is because in packed-bed discharges, the area of the dielectric surface is much

larger than inside the pores, and the sidewalls of the pores at opposite sides are so close to each other then they can counteract, thus affecting the plasma behavior. Therefore, we look forward to experiments validating our results in the future.

The electron temperature (Fig. 7(b)) seems to be always higher inside the pore than in the sheath near the top dielectric, for all pore sizes and dielectric constants investigated (except for $\varepsilon_r = 1000$ and the 10 μm pore), but because the electron density is not always enhanced inside the pore, the ionization rate, which is determined by both, is only enhanced for the smaller dielectric constants, where the electron temperature inside the pore is significantly higher than in the sheath in front of the top dielectric.

Finally, the ion density inside the pore is only enhanced for the pore sizes of 100 μm, 50 μm and 30 μm, and again only for a limited range of dielectric constants, being smaller for the smaller pore sizes. The transition point (below or equal to which the ion density inside the pore is larger than in the sheath near the top dielectric) occurs at $\varepsilon_r = 300$, 150 and 75 for the 100 μm, 50 μm and 30 μm pores. When the pore size is 10 μm, the ion density in the sheath is always higher than inside the pore, except for $\varepsilon_r = 4$. Indeed, the plasma generation is limited in the 10 μm pore under these conditions. Therefore, it is clear that both the pore size and the dielectric constant of the material greatly affect the plasma characteristics, and play a significant role in determining whether microdischarges can be formed inside catalyst pores.

4. Conclusions

In this work, we investigated the influence of the dielectric constant of the catalytic or support material on the plasma properties, and especially on the microdischarge formation inside catalyst pores, by means of a two-dimensional fluid model for a helium atmospheric dielectric barrier discharge. We first studied in detail the plasma behavior in a 100 μm pore for different dielectric constants, ranging from $\varepsilon_r = 4$ to $\varepsilon_r = 1000$. We find that the ionization

is significantly enhanced inside the pore for dielectric constants below 200. As the dielectric constant becomes larger, the ionization rate inside the pore decreases dramatically, whereas it increases in the sheath in front of the bottom dielectric, but the maximum still appears inside and above the pore at $\varepsilon_r = 300$. When the dielectric constant increases further to $\varepsilon_r = 1000$, the ionization reaches its maximum in the sheath and the ionization inside the pore is negligible. This is because the dielectric material is more effectively polarized for larger dielectric constants, and this gives rise to a stronger local electric field in the sheath near the dielectric, which is consistent with the high density of the potential contour lines outside the pore above the bottom dielectric. This strong electric field in the sheath leads to the high electron temperature, and accordingly results in enhanced ionization in the sheath. Inside the pore, the electric field is slightly enhanced when the dielectric constant increases from $\varepsilon_r = 4$ to $\varepsilon_r = 25$. For larger dielectric constants, the polarization of the left sidewall counteracts that of the right sidewall, and thus the electric field is reduced. Especially for $\varepsilon_r = 1000$, the potential only drops slightly inside the pore. Therefore, this weak electric field results in a low electron temperature and significantly limits the plasma generation inside the pore for very high dielectric constants.

We have also studied the evolution of the plasma properties inside the pore and in the sheath near the top dielectric with changing dielectric constant and for various pore sizes. For pore sizes above 30 μm, the averaged ionization rate inside the pore first increases with dielectric constant, and then decreases, due to the similar behavior of the electron temperature and electric field. As a result, the maximum of the ion density appears at $\varepsilon_r = 25$. However, for a 10 μm pore, the ionization rate and the electron temperature decrease monotonically with dielectric constant, because the counteraction of the polarization of both sidewalls is pronounced even for a small dielectric constant, due to the small gap. Moreover, the ion

density inside a 10 μm pore first decreases with dielectric constant due to the lower ionization rate, and then it increases slightly because less ions are lost at the sidewalls.

By comparing the plasma properties inside the pore with those in the sheath for the various pore sizes and dielectric constants, we can conclude that the ionization rate inside a 100 μm pore (being characteristic for the microdischarge generation inside the pore) is higher than in the sheath for dielectric constants below $\varepsilon_r = 300$, while the smaller pores only yield enhanced ionization for smaller dielectric constants. Indeed, the transition points, below or equal to which the ionization rate inside the pore is larger than in the sheath near the top dielectric, occur at $\varepsilon_r = 200$, $\varepsilon_r = 150$ and $\varepsilon_r = 50$ for the 50 μm, 30 μm and 10 μm pores, respectively. Note that $\varepsilon_r = 300$ is a typical value for $SrTiO_3$, $\varepsilon_r = 200$ corresponds to $CaTiO_3$, and $\varepsilon_r = 50$ is a typical value for TiO_2 [19]. The most commonly used catalyst supports, like Al_2O_3 and SiO_2, have lower dielectric constants i.e., around ε_r = 8-11 and 4.2, respectively, so they should allow more easily microdischarge formation inside catalyst pores, even for smaller pore sizes. On the other hand, our calculations reveal that ferroelectric materials with dielectric constants above $\varepsilon_r = 300$ never yield plasma enhancement inside catalyst pores, even not for 100 μm pore sizes. Although some experiments are performed in discharges with different ferroelectric packed-bed materials, to our knowledge, no experiments are available for the different plasma behavior inside catalyst pores with different dielectric constants. This behavior is probably different from that in between the beads of packed-bed discharges. Therefore, we look forward to experiments validating our results in the future.

In conclusion, our model predicts that the plasma generation inside larger pores is enhanced for a wider range of dielectric constants, while the plasma generation inside smaller pores is more limited to lower dielectric constants. In general, it is clear that the dielectric constant of the material has a large effect on the extent of plasma enhancement inside the catalyst pores, especially in the range between $\varepsilon_r = 4$ and $\varepsilon_r = 200$. These model results are of significant

importance for plasma catalysis, as the availability of reactive species inside catalyst pores might affect its morphology and work function, especially gives rise to larger active surface area that is available for surface reactions, and thus improve the catalyst performance in practical applications.

Acknowledgments

This work was supported by the Fund for Scientific Research Flanders (FWO) (Grant No. G.0217.14N), the National Natural Science Foundation of China (Grant No. 11405019), and the China Postdoctoral Science Foundation (Grant No. 2015T80244). This work was carried out in part using the Turing HPC infrastructure at the CalcUA core facility of the Universiteit Antwerpen, a division of the Flemish Supercomputer Center VSC, funded by the Hercules Foundation, the Flemish Government (department EWI) and the University of Antwerp.

References

[1] Neyts, E. C.; Ostrikov, K.; Sunkara, M. K.; Bogaerts, A. Chem. Rev. 2015, 115, 13408.

[2] Neyts, E. C.; Bogaerts, A. J. Phys. D: Appl. Phys. 2014, 47, 224010.

[3] Whitehead, J. C. Pure Appl. Chem. 2010, 82, 1329.

[4] Chen, H. L.; Lee, H. M.; Chen, S. H.; Chang, M. B.; Yu, S. J.; Li, S. N. Env. Sci. Technol. 2009, 43, 2216.

[5] Chen, H. L.; Lee, H. M.; Chen, S. H.; Chao, Y.; Chang, M. B. Appl. Catal. B: Environ. 2008, 85, 1.

[6] Van Durme, J.; Dewulf, J.; Leys, C.; Van Langenhove, H. Appl. Catal. B: Environ. 2008, 78, 324.

[7] Neyts, E. C. Plasma Chem. Plasma Process. 2016, 36, 185.

[8] Pylinina, A. I.; Mikhalenko, I. I. Theor. Exp. Chem. 2013, 49, 65.

[9] Demidyuk, V.; Whitehead, J. C. Plasma Chem. Plasma Process. 2007, 27, 85.

[10] Guo, Y. F.; Ye, D. Q.; Chen, K. F.; He, J. C.; Chen, W. L. J. Mol. Catal. A 2006, 245, 93.

[11] Liu, C. J.; Mallison, R.; Lobban, L. J. Catal. 1998, 179, 326.

[12] Wu, C. C.; Wu, C. I.; Sturm, J. C.; Kahn, A. Appl. Phys. Lett. 1997, 70, 1348.

[13] Rousseau, A.; Guaitella, O.; Ropcke, J.; GatilovaL, V.; Tolmachev, Y. A. Appl. Phys. Lett. 2004, 85, 2199.

[14] Kang, W. S.; Park, J. M.; Kim, Y.; Hong, S. H. IEEE Trans. Plasma Sci. 2003, 31, 504.

[15] Chang, J. S.; Kostov, K. G.; Urashima, K.; Yamamoto, T.; Okayasu, Y.; Kato, T.; Iwaizumi, T.; Yoshimura, K. IEEE Trans. Ind. Appl. 2000, 36, 1251.

[16] Ogata, A.; Ito, D.; Mizuno, K.; Kushiyama, S.; Yamamoto, T. IEEE Trans. Ind. Appl. 2001, 37, 959.

[17] Takuma, T. IEEE Trans. Electr. Insul. 1991, 26, 500.

[18] Mei, D.; Zhu. X.; Wu, C.; Ashford, B.; Williams, P. T.; Tu, X. Appl. Catal. B: Environ. 2016, 182, 525.

[19] Kim, H. H.; Teramoto, Y.; Negishi, N; Ogata, A. Catal. Today 2015, 256, 13.

[20] Gallon, H. J.; Tu, X.; Whitehead, J. C. Plasma Proc. Polym. 2012, 9, 90.

[21] Tu, X.; Whitehead, J. C. Appl. Catal. B: Environ. 2012, 125, 439.

[22] Kim, H. H.; Ogata, A. Eur. Phys. J. Appl. Phys. 2011, 55, 13806.

[23] Tu, X.; Gallon, H. J.; Twigg, M. V.; Gorry, P. A.; Whitehead, J. C. J. Phys. D: Appl. Phys. 2011, 44, 274007.

[24] Kim, H. H.; Ogata, A.; Futamura, S. Appl. Catal. B: Environ. 2008, 79, 356.

[25] Wang, H.; Li, J.; Quan, X.; Wu, Y. Appl. Catal. B: Environ. 2008, 83, 72.

[26] Nozaki, T.; Muto, N.; Kado, S.; Okazaki, K. Catal. Today 2004, 89, 57.

[27] Holzer, F.; Roland, U.; Kopinke, F. D. Appl. Catal. B: Environ. 2002, 38, 163.

[28] Roland, U.; Holzer, F.; Kopinke, F. D. Appl. Catal. B: Environ. 2005, 58, 217.

[29] Holzer, F.; Kopinke, F. D.; Roland, U. Plasma Chem. Plasma Process. 2005, 25, 595.

[30] Hensel, K.; Katsura, S.; Mizuno, A. IEEE Trans. Plasma Sci. 2005, 33, 574.

[31] Hensel, K.; Martisovits, V.; Machala, Z.; Janda, M.; Lestinsky, M.; Tardiveau, P.; Mizuno, A. Plasma Process. Polym. 2007, 4, 682.

[32] Hensel, K. Eur. Phys. J. D 2009, 54, 141.

[33] Zhang, Y. R.; Van Laer, K.; Neyts, E. C.; Bogaerts, A. Appl. Catal. B: Environ. 2016, 185, 56.

[34] Mizuno, A.; Ito, H. J. Electrostat. 1990, 25, 97.

[35] Roland, U.; Holzer, F.; Kopinke, F. D. Catal. Today 2002, 73, 315.

[36] Takaki, K.; Chang, J. S.; Kostov, K. G. IEEE T. Dielect. El. In. 2004, 11, 481.

[37] Jo, S.; Kim, T.; Lee, D. H.; Kang, W. S.; Song, Y. H. Plasma Chem. Plasma Process. 2014, 34, 175.

[38] Van Laer, K.; Bogaerts, A. Plasma Sources Sci. Technol. 2016, 25, 015002.

[39] Zhang, Y.; Wang, H. Y.; Jiang, W.; Bogaerts, A. New J. Phys. 2015, 17, 083056.

[40] Comsol Website; http://www.comsol.com

[41] Yokoyama, T.; Kogoma, M.; Moriwaki, T.; Okazaki, S. J. Phys. D: Appl. Phys. 1990, 23, 1125.

[42] Van Laer, K.; Bogaerts, A. Energy Technol. 2015, 3, 1038.

[43] Hagelaar, G. J. M.; Pitchford, L. C. Plasma Sources Sci. Technol. 2005, 14, 722.

[44] Patterson, P. L. Phys. Rev. A 1970, 2, 1154.

[45] Morgan database, www.lxcat.net, retrieved on July 25, 2013

[46] Martens, T.; Bogaerts, A.; Brok, W.; van Dijk, J. Anal. Bioanal. Chem. 2007, 288, 1583.

[47] Wang, Q.; Economou, D. J.; Donnelly, V. M. J. Appl. Phys. 2006, 100, 023301.

Figure Captions

Fig. 1 Geometry used in the model.

Fig. 2 Distributions of the electron impact ionization rate, averaged over time in 1 AC cycle, for different dielectric constants: (a) $\varepsilon_r = 25$, (b) $\varepsilon_r = 300$, (c) $\varepsilon_r = 400$, (d) $\varepsilon_r = 1000$, for a helium discharge sustained at 20 kV with a 100 μm pore.

Fig. 3 Distributions of the electron temperature, averaged over time in 1 AC cycle, for different dielectric constants: (a) $\varepsilon_r = 25$, (b) $\varepsilon_r = 300$, (c) $\varepsilon_r = 400$, (d) $\varepsilon_r = 1000$, for a helium discharge sustained at 20 kV with a 100 μm pore.

Fig. 4 Distributions of the electron impact ionization rate (a), electron temperature (b), electron density (c) and total ion density (d) along the vertical centerline from the bottom of the pore to the top dielectric surface, for different dielectric constants, for a helium discharge sustained at 20 kV with a 100 μm pore.

Fig.5 Distributions of the potential, averaged over time in 1 AC cycle, for different dielectric constants: (a) $\varepsilon_r = 25$, (b) $\varepsilon_r = 300$, (c) $\varepsilon_r = 400$, (d) $\varepsilon_r = 1000$, for a helium discharge sustained at 20 kV with a 100 μm pore.

Fig.6 Distributions of the surface charge density, averaged over time in 1 AC cycle, at the dielectric surface outside of the pore (regions A and E), the pore sidewalls (regions B and D) and the pore bottom (region C), for different dielectric constants, for a helium discharge sustained at 20 kV with a 100 μm pore.

Fig.7 Averaged electron impact ionization rate (a), electron temperature (b) and total ion density (c) inside the pore (solid lines with close symbols) and in the sheath near the top dielectric (dashed lines with open symbols), as a function of dielectric constant for different pore sizes, for a helium discharge sustained at 20 kV.

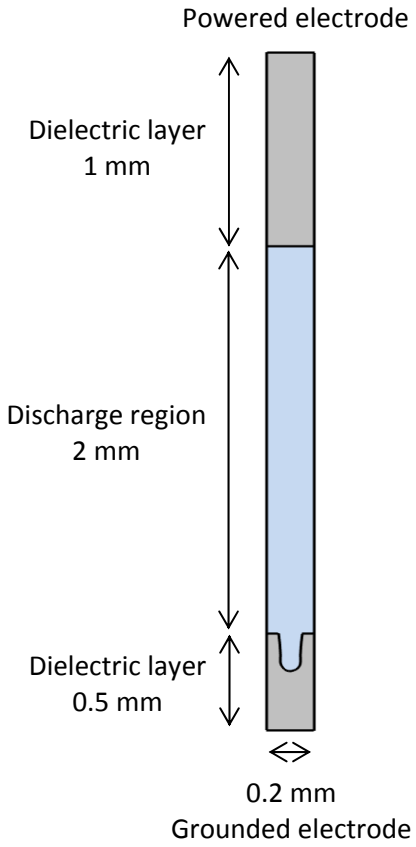
Powered electrode
Dielectric layer
1 mm
Discharge region
2 mm
Dielectric layer
0.5 mm
0.2 mm
Grounded electrode

Figure 1

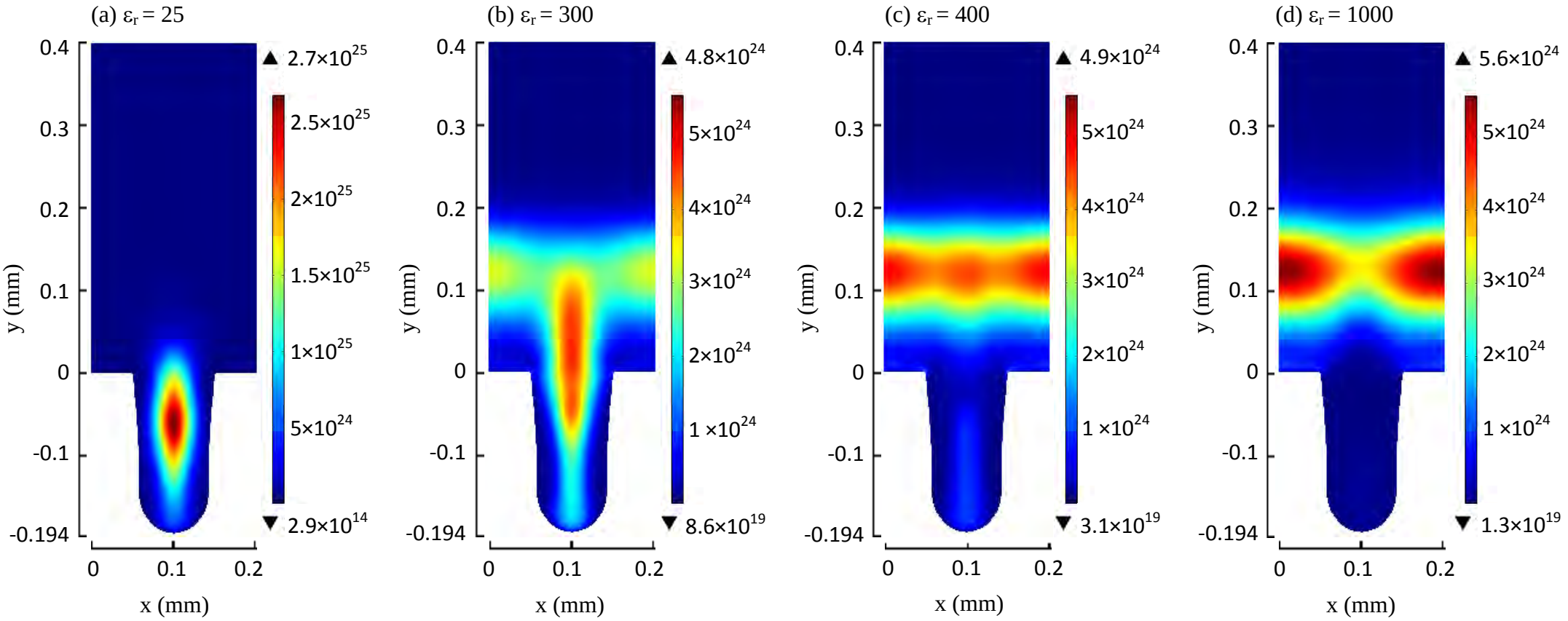
(a) εr = 25
(b) εr = 300
(c) εr = 400
(d) εr = 1000
y (mm)
x (mm)
0.4
0.3
0.2
0.1
0
-0.1
-0.194
0
0.1
0.2
▲ 2.7×10^25
2.5×10^25
2×10^25
1.5×10^25
1×10^25
5×10^24
▼ 2.9×10^14
▲ 4.8×10^24
5×10^24
4×10^24
3×10^24
2×10^24
1 ×10^24
▼ 8.6×10^19
▲ 4.9×10^24
5×10^24
4×10^24
3×10^24
2×10^24
1 ×10^24
▼ 3.1×10^19
▲ 5.6×10^24
5×10^24
4×10^24
3×10^24
2×10^24
1 ×10^24
▼ 1.3×10^19

Figure 2

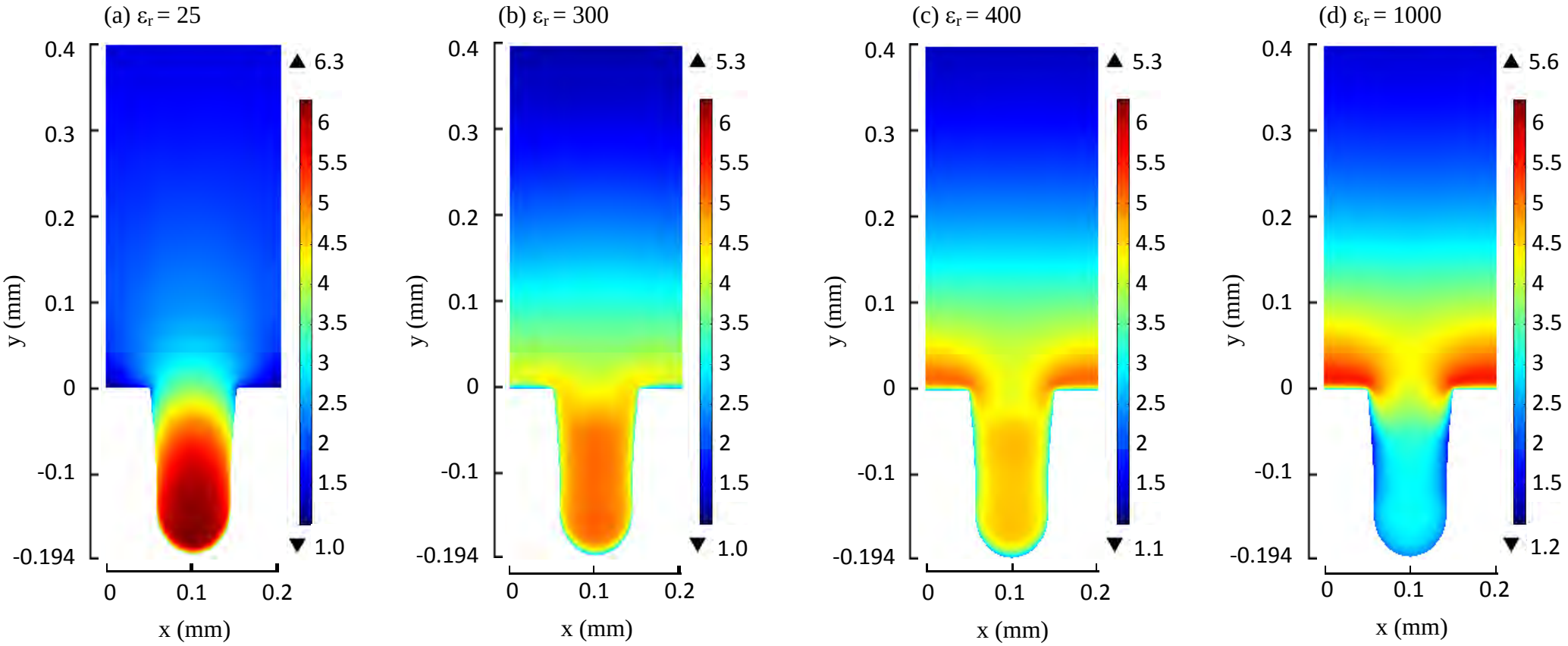
(a) ε_r = 25
(b) ε_r = 300
(c) ε_r = 400
(d) ε_r = 1000
y (mm)
x (mm)
0.4
0.3
0.2
0.1
0
-0.1
-0.194
0
0.1
0.2
▲ 6.3
▲ 5.3
▲ 5.3
▲ 5.6
6
5.5
5
4.5
4
3.5
3
2.5
2
1.5
▼ 1.0
▼ 1.0
▼ 1.1
▼ 1.2

Figure 3

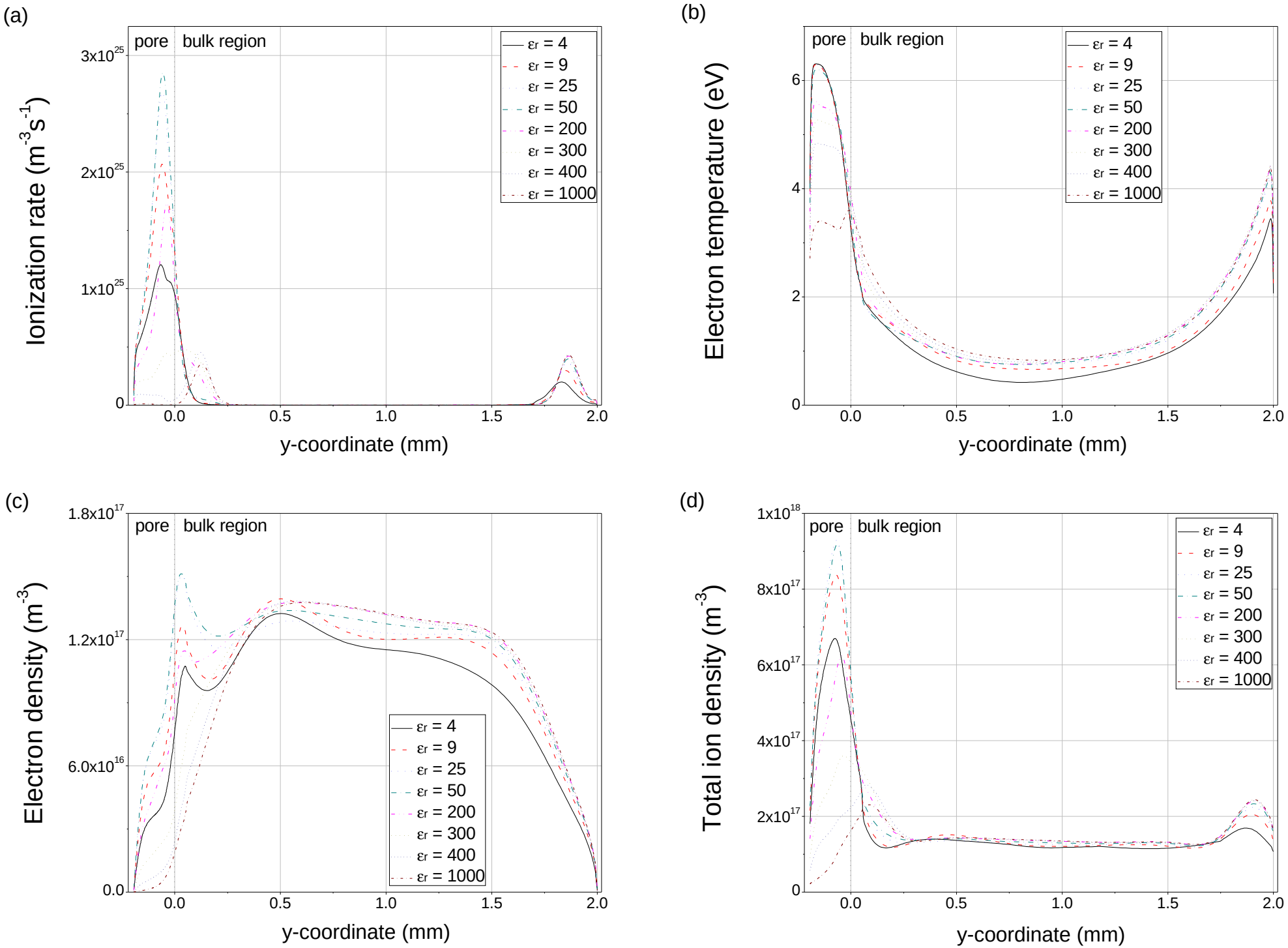
(a)
pore
bulk region
Ionization rate (m-3s-1)
3x10^25
2x10^25
1x10^25
0
0.0
0.5
1.0
1.5
2.0
y-coordinate (mm)
εr = 4
εr = 9
εr = 25
εr = 50
εr = 200
εr = 300
εr = 400
εr = 1000
(b)
pore
bulk region
Electron temperature (eV)
6
4
2
0
0.0
0.5
1.0
1.5
2.0
y-coordinate (mm)
εr = 4
εr = 9
εr = 25
εr = 50
εr = 200
εr = 300
εr = 400
εr = 1000
(c)
pore
bulk region
Electron density (m-3)
1.8x10^17
1.2x10^17
6.0x10^16
0.0
0.0
0.5
1.0
1.5
2.0
y-coordinate (mm)
εr = 4
εr = 9
εr = 25
εr = 50
εr = 200
εr = 300
εr = 400
εr = 1000
(d)
pore
bulk region
Total ion density (m-3)
1x10^18
8x10^17
6x10^17
4x10^17
2x10^17
0
0.0
0.5
1.0
1.5
2.0
y-coordinate (mm)
εr = 4
εr = 9
εr = 25
εr = 50
εr = 200
εr = 300
εr = 400
εr = 1000

Figure 4

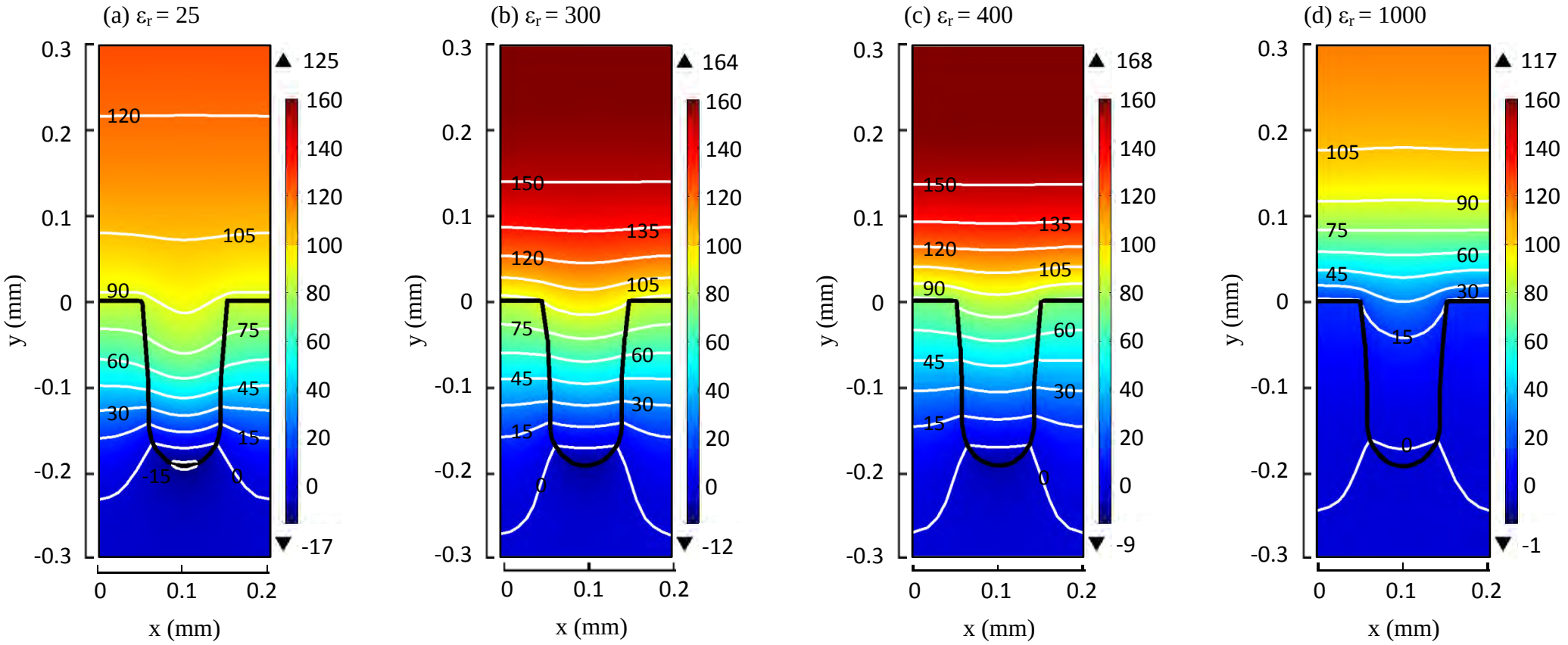
(a) ε_r = 25
(b) ε_r = 300
(c) ε_r = 400
(d) ε_r = 1000
y (mm)
x (mm)
0.3
0.2
0.1
0
-0.1
-0.2
-0.3
0
0.1
0.2
125
164
168
117
160
140
120
100
80
60
40
20
0
-17
-12
-9
-1
120
105
90
75
60
45
30
15
0
-15
150
135

Figure 5

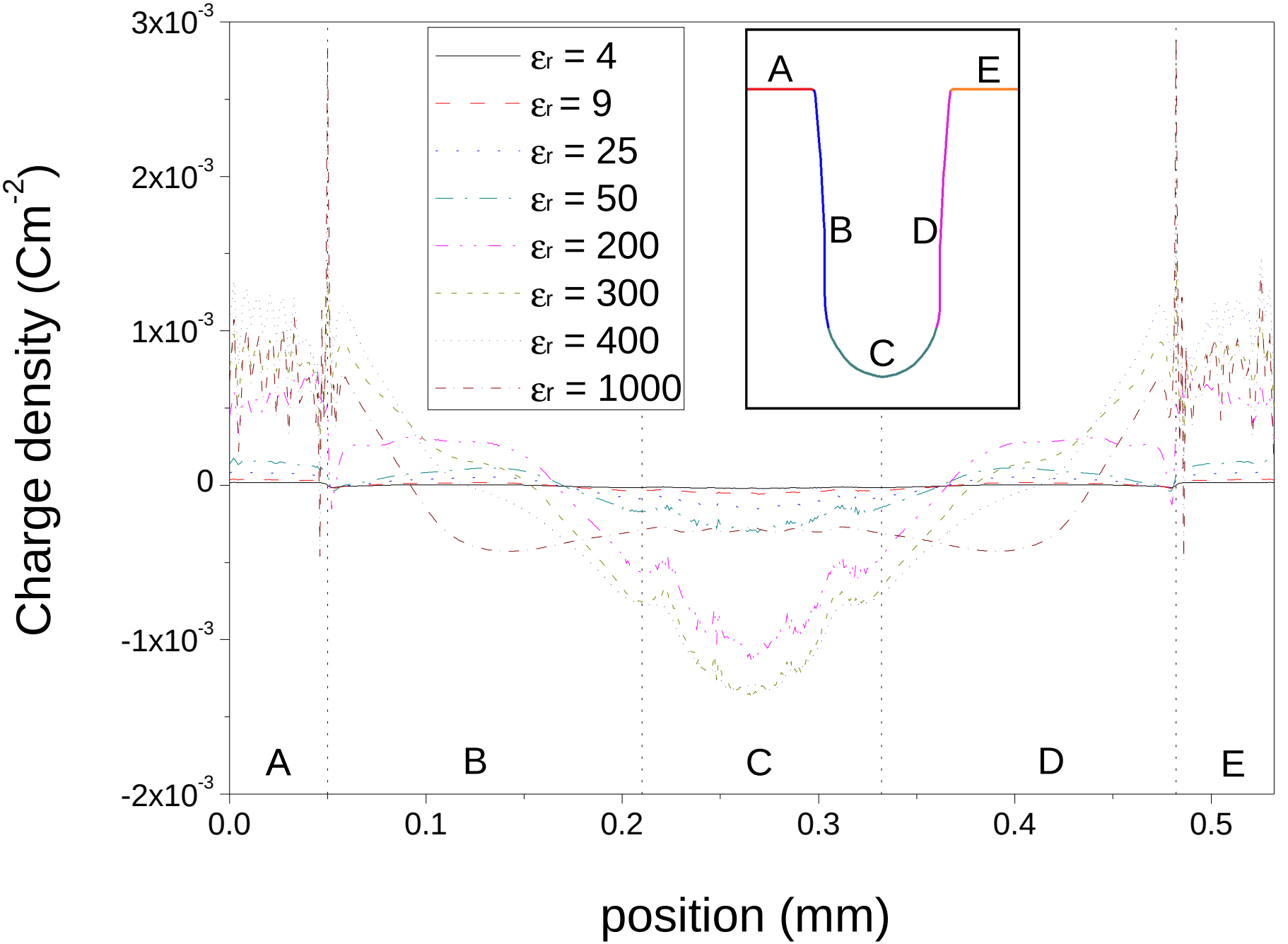
Charge density (Cm-2)
3x10-3
2x10-3
1x10-3
0
-1x10-3
-2x10-3
0.0
0.1
0.2
0.3
0.4
0.5
position (mm)
εr = 4
εr = 9
εr = 25
εr = 50
εr = 200
εr = 300
εr = 400
εr = 1000
A
B
C
D
E

Figure 6

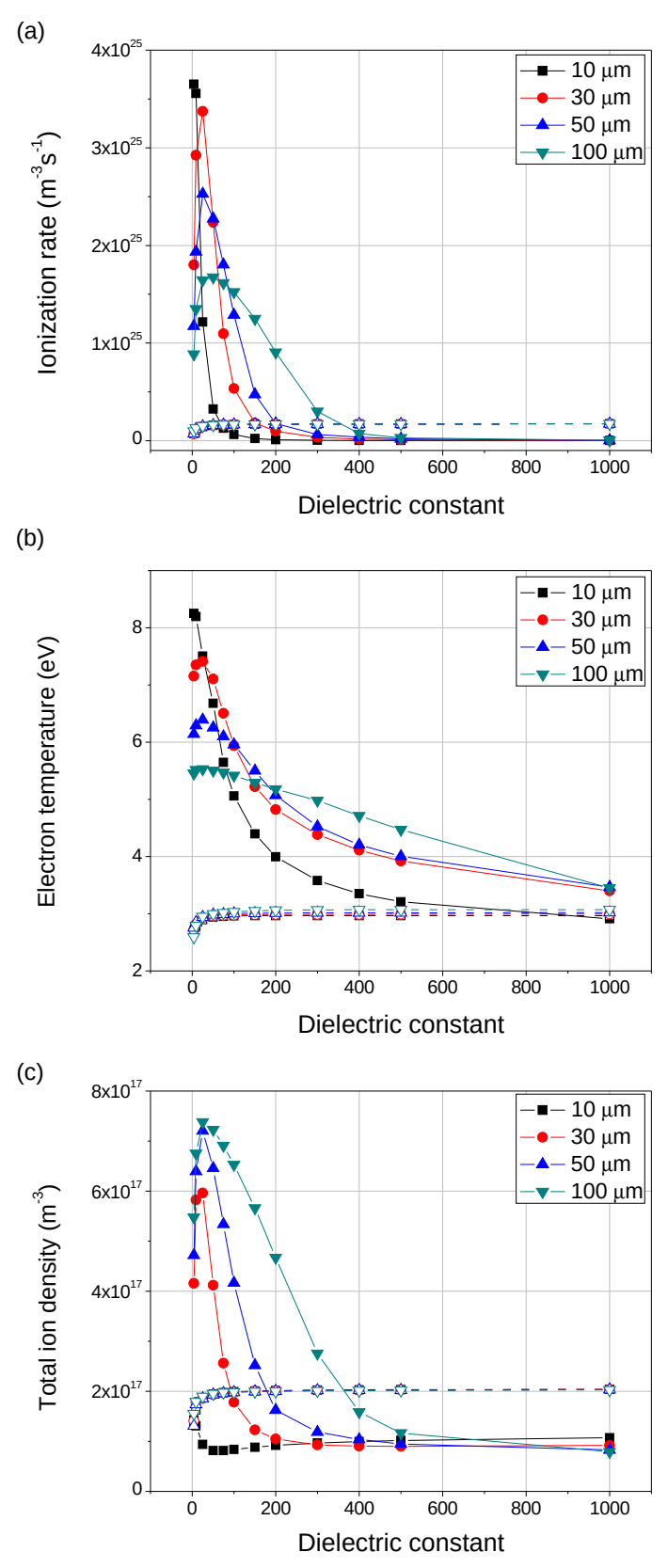
(a)
Ionization rate (m-3s-1)
4x10^25
3x10^25
2x10^25
1x10^25
0
0
200
400
600
800
1000
Dielectric constant
10 μm
30 μm
50 μm
100 μm
(b)
Electron temperature (eV)
8
6
4
2
0
200
400
600
800
1000
Dielectric constant
10 μm
30 μm
50 μm
100 μm
(c)
Total ion density (m-3)
8x10^17
6x10^17
4x10^17
2x10^17
0
0
200
400
600
800
1000
Dielectric constant
10 μm
30 μm
50 μm
100 μm

Figure 7